Supporting Information

Mao et al. 10.1073/pnas.1114319109

SI Text

Selection of Fossil Taxa and Their Phylogenetic Positions. The integration of fossil calibrations is the most critical step in molecular dating (1, 2). We only used the fossil taxa with ovulate cones that could be assigned unambiguously to the extant groups (Table S4). The exact phylogenetic position of fossils used to calibrate the molecular clocks was determined using the total-evidence analyses (following refs. 3–5). *Cordaixylon iowensis* was not included in the analyses because its assignment to the crown Acrogymnospermae already is supported by previous cladistic analyses (also using the total-evidence approach) (6). Two data matrices were compiled. Matrix A comprised *Ginkgo biloba*, 12 living representatives from each conifer family, and three fossils taxa related to Pinaceae and Araucariaceae (16 taxa in total; Fig. S5*A*). In this matrix, the 105 morphological characters and their states follow Gernandt et al. (ref. 7 and references therein). Matrix B comprised *Pinus sylvestris*, *Sciadopitys verticillata*, 39 living taxa, and 17 fossil taxa that are closely related to Cupressaceae (58 taxa in total). In this matrix, the 53 morphological characters and their states follow Farjon (8) and two updates (9-10). Both data matrices include 5,476 molecular characters for all living taxa extracted from the plastid DNA sequence matrix (144-taxon dataset), with the fossil taxa coded as having "missing data." Molecular and morphological characters were concatenated in both matrices, and parsimony analyses were performed using the program TNT 1.1 (11), with heuristic searching based on 5,000 random addition sequences and Tree-Bisection-Reconnection swapping (saving 10 trees per replication). All shortest trees were saved and summarized into a strict consensus tree. All characters were weighted equally, and the resulting phylogenetic trees were rooted on *Ginkgo biloba* (matrix A) (Fig. S5*A*) or on *Pinus sylvestris* (matrix B) (Fig. S5 *B–I*).

As shown in Fig. S5*A*, Matrix A yielded a tree in which the phylogenetic positions of the fossil taxa were well resolved. Matrix B, however, yielded a tree in which phylogenetic positions of more than half of the fossil taxa were unresolved. We then ran a series of analyses, each of which included a different subset of fossils, and determined that seven fossils (*Hughmillerites juddii*, *Athrotaxis ungeri*, *Austrosequoia wintonensis*, *Glyptostrobus* sp., *Papuacedrus prechilensis*, *Thuja polaris*, and *Fokienia ravenscragensis*) are responsible for the collapsing of the tree, likely because that fewer morphological characters are available for them than for the others included in Matrix B. We therefore determined the position of the other 10 fossils by reanalyzing Matrix B with only these 10 fossils included (Fig. S5*I*). We further studied the placement of each of the seven problematic fossils by analyzing a version of Matrix B containing only one target fossil alongside all the living taxa (Fig. S5 *B–H*). All data matrices and resulting trees have been submitted to TreeBASE (study accession no. S12554).

Cross-validation tests of the different fossil calibrations (Fig. S7 and ref. 12) were performed with the program R8S under Penalized Likelihood rate smoothing using the 56-taxon dataset. A maximum constraint was used only for calibration P while the remaining 16 calibrations used the minimum constraints (Fig. S7 and Table S4). Only the calibration Wa (*Widdringtonia americana*) (13) resulted in the node ages significantly older than those of the other fossil calibrations (Fig. S7). This fossil appears to be wrongly placed in the living genus *Widdringtonia*, as suggested also by Crisp and Cook (14). We therefore excluded the calibration Wa from further analyses.

BEAST Analyses. In addition to a BEAST analysis that used uniform prior distributions for all calibrations (run 1; 144-taxon dataset, calibrations as in Table S4), we performed eight additional analyses to explore factors affecting estimates of divergence time (Fig. S3).

First, to test the effect of calibration point P, which is close to the root node and is the only functional hard maximum constraint in BEAST runs using uniform priors, we carried out three runs with calibrations A through O (Table S4), and calibration P set to [306.2, 351.7] (run 2), [306.2, 336.5] (run 3), and [306.2, 321.4] (run 4). The age estimates obtained in runs 2, 3, and 4 largely overlapped with those from run 1 (Fig. S3).

Second, we carried out two runs with different subsets of calibrations using uniform priors. When parsing the log.txt file of run 1 with Tracer 1.4 (15), we noted that the posterior distribution of nodes calibrated with the minimum constraints (calibrations A through O) fell into two groups. One included calibrations C, D, H, I, M, N, and O. For each node calibrated with these fossils (Table S4), the posterior distributions of their age estimates significantly violated a normal distribution (hence our name for this subset: "VND"). The other group included calibrations A, B, E, F, G, J, K, and L. For each node calibrated with these fossils (Table S4), the posterior distributions of their age estimates did not significantly violate a normal distribution (hence, subset "NVND"). When comparing between-lineage age estimates derived from BEAST runs based on calibration subset VND (plus calibration P) (run 5) and subset NVND (plus calibration P) (run 6), we found that the calibration subset NVND (run 6) significantly underestimated lineage ages when compared with the calibration subset VND (run5) or the calibrations A through P (run 1) (Fig. S3).

Third, we carried out another BEAST run that incorporated lognormal priors. Calibrations that may underestimate lineage age should not be given lognormal priors, because a lognormal prior places a rapidly declining probability on older ages (16). Nevertheless, fossils that underestimate lineage ages still may be useful as hard minimum constraints, as suggested by previous studies (12, 17, 18). For this reason, uniform priors were retained for the subset NVND, whereas lognormal priors were applied for the calibration P and the subset VND (run 7) (see Table S4). The age estimates obtained in run 7 largely overlapped with those from runs 1 and 5 (Fig. S3). However, one run (with lognormal priors; run 7) bias to estimate the node ages younger and another run (with uniform priors; run 1) bias to estimate the node ages older, so "the truth is likely to be somewhere in between" (19).

Fourth, we also carried out a run that included *Widdringtonia americana* (calibration Wa) as a hard minimum calibration in addition to calibrations A through P (run 8). Integration of this calibration resulted in significantly older age estimates for nodes 1–10 (Fig. S3), demonstrating that the calibration Wa has a potential to overestimate lineage ages. As suggested by the cross-validation test and a recent study (14), it is better to exclude the calibration Wa.

Finally, we carried out a BEAST run on the 56-taxon matrix that assumed uniform prior for all calibrations (run 9) (Table S4). The ages obtained are slightly younger than these obtained with 144-taxon matrix (Fig. S3). This result is consistent with the effects of undersampling observed elsewhere (20).

Ancestral Area Reconstruction. Ancestral area reconstruction (AAR) under the dispersal-extinction-cladogenesis model, as implemented in LAGRANGE (21), requires a matrix that defines

migration probabilities among the six operational geographic areas (see Fig. 2*A* for their boundaries). Migration probabilities among areas were based on geological history, climate history, and the presence and dissolution of land bridges and island chains. Geological events considered were the presence of a land connection between all operational area before the break-up of Pangea, the separation between Laurasia and Gondwana, the gradual fragmentation of Gondwana and Laurasia, island chains between North and South America, the collision of Australian and Asian plates, and the collision of African and Asian plates (22-26). Migration probabilities range from 0.1 for well-separated areas to 1.0 for contiguous landmasses (Table S6), and the LAGRANGE online configuration tool (21) was used to devise a matrix that reflected different migration probabilities between areas at different periods (i.e., time slices) in the past. Based on plate tectonics, we defined eight area pairs and one area combination as ancestral area candidates in AAR analyses: NS, NE, SF, NA, AE, FE, SU, NF, and NAE (in which "E" stands for Europe, north Africa, and northern Arabia; "A" represents Asia; "N" represents North America, Caribbean, and Central America; "S" represents South America; "F" represents south to middle Africa and southern Arabia; and "U" represents Australia, New Guinea, New Caledonia, and New Zealand). Because the connectivity between our six operational geographic units changed during the past 275 million years, we decided to develop a time-slice model that would reflect changing continental connectivity. To find the best-fitting time-slice model, we compared models with five time slices (275–160 Ma, 160–125 Ma, 125–70 Ma, 70–30 Ma, and 30 Ma to the present), six time slices (275–160 Ma, 160–125 Ma, 125–105 Ma, 105–70 Ma, 70–30 Ma, and 30 Ma to the present), seven time slices (275–160 Ma, 160–125 Ma, 125–105 Ma, 105–70 Ma, 70–45 Ma, 45–30 Ma, and 30 Ma to the present), and eight time slices (275–160 Ma, 160–125 Ma, 125–105 Ma, 105–70 Ma, 70–45 Ma, 45–30 Ma, 30–5 Ma, and 5 Ma to the present). For each of these four time-slice schemes, we compiled a separate migration probability matrix and calculated its global maximum likelihood in LAGRANGE. Comparison of the resulting global likelihoods suggested that the eight-time-slice matrix (Table S6) fit our data best, and we therefore adopted this migration probability matrix for all subsequent AAR analyses.

We performed additional AAR analyses on trees that comprised 29 fossils or groups of fossils representing extinct taxa (Fig. 2 *C–E*, Fig. S4, and Table S5) (26, 27), the 122 sequenced living taxa of Cupressaceae and four outgroups. For these analyses, fossils were placed as extinct sister lineages to those living lineages with which they showed the closest morphological affinities as assessed in their original publications and related updates (for detailed placement justifications, see Table S5). The divergence between extinct lineages and their sister lineages (living taxa) was determined based on the earliest fossil of each extinct lineage (always determined as the youngest possible age of the formation or stratum in which a fossil occurred). For the absolute age of each geological stratum, we relied on the latest geologic time scale (28).

As shown in Fig. 2 and Fig. S4, our AARs inferred four types of events affecting geographic ranges of either living or extinct lineages. First, instances of dispersal result in range expansion (indicated by black arrows on a lineage); such events are common throughout the Cupressaceae tree. Second, local extinction events (indicated by a red "X" on a lineage; 11 are hypothesized in Fig. S4) are inferred when a daughter lineage (*i*) inherits a range different from that of its parent (a range expansion before local extinction is inferred; 10 such events are hypothesized in Fig. S4) or (*ii*) inherits a reduced range relative to its parent (one instance related to *Metasequoia* is hypothesized in Fig. 2 *C–E* and in Fig. S4). Third, cladogenesis events caused by vicariance (indicated by blue arrows on a lineage) are inferred where the ancestral range encompassing two or more areas subdivides between daughter lineages. Fourth, a combination of range expansion and subsequent cladogenesis caused by vicariance is inferred when one daughter lineage inherits the range of its parent, and the other inherits a different range (e.g., the separation between *Athrotaxites berryi* and *Athrotaxis* in Fig. 2 *C–E*). Note that each of the fossil taxa shown by dashed lines in Fig. 2 and Fig. S4 experienced one extra total extinction event compared with living taxa shown by solid lines.

Our total-evidence analyses fully resolved the phylogenetic position of *Athrotaxites berryi* and partly resolved the phylogenetic positions of *Austrohamia minuta*, *Austrohamia acanthobractea*, and *Sewardiodendron laxum* (Fig. S5*I*) but failed for *Hughmillerites juddii* (Fig. S5*B*). We therefore excluded *Hughmillerites juddii* from AAR analyses (its inclusion resulted in the collapse of the Cupressaceae phylogenetic tree: Fig. S5*B*). To include *Austrohamia minuta*, *Austrohamia acanthobractea*, and *Sewardiodendron laxum* in the AARs, we assigned them to three possible placement scenarios and performed likelihood AARs for each scenario. As shown in Fig. 2 *C–E*, *A. minuta* and *A. acanthobractea* always were assumed to be sister to each other. Scenario 1 (Fig. 2*C*) assumes that *Sewardiodendron* diverged from Cunninghamioideae (both living and extinct members) (Fig. 2 and Fig. S4) at 157.2 Ma, and both of them share a most recent common ancestor (MRCA) with *Austrohamia* at 164.2 Ma. Scenario 2 (Fig. 2*D*) assumed that *Sewardiodendron* and *Austrohamia* shared a MRCA at 157.2 Ma and diverged from Cunninghamioideae 164.2 Ma. Scenario 3 (Fig. 2*E*) assumed that *Sewardiodendron* and *Austrohamia* shared a MRCA at 164.2 Ma and diverged from the MRCA of all Cupressaceae subfamilies except Cunninghamioideae at 211.5 Ma (the intermediate age between nodes 2 and 3 in Table 1).

Diversification Modeling. Using the TreeSim R package (29) and the BEAST highest posterior probability chronogram obtained for the Cupressaceae (from the 144-taxon dataset) as input, we simulated 1,000 trees with the number of tips corresponding to the total number of extant species of Cupressaceae (162 species) and speciation and extinction rates obtained by fitting the constant rate birth-death model to the chronogram. To add the 40 extant species that were not sequenced, we used the sim.missing function in the CorSiM R package (30) and simulated 1,000 trees under a constant-rate birth-death model, assuming that the missing speciation events are not distributed randomly over the tree but probably happened during the past 10 million years. We then applied birth/death likelihood (BDL) analysis (using TreePar) to the 1,000 completed trees to obtain means and SDs for the γ statistic, the Akaike information criterion values, and the inferred rate parameters from the BDL analyses. TreePar also calculates the percentage of trees to which a particular model fits best. Among the five models under comparison (CR-PB, constant-rate birth-death, logistic density dependence, exponential density dependence, and a two-rate variant of the pure-birth model with a rate shift at a certain time point), the two-rate model provided the best fit for all 1,000 trees. The CR-PB provided the second-best fit.

1. Clarke JT, Warnock RC, Donoghue PC (2011) Establishing a time-scale for plant evolution. *New Phytol* 192:266–301.
2. Hedges SB, Kumar S (2004) Precision of molecular time estimates. *Trends Genet* 20: 242–247.
3. Sun G, et al. (2002) Archaefructaceae, a new basal angiosperm family. *Science* 296:899–904.
4. Peterson KJ, Butterfield NJ (2005) Origin of the Eumetazoa: Testing ecological predictions of molecular clocks against the Proterozoic fossil record. *Proc Natl Acad Sci USA* 102:9547–9552.
5. Manos PS, et al. (2007) Phylogeny of extant and fossil Juglandaceae inferred from the integration of molecular and morphological data sets. *Syst Biol* 56:412–430.

6. Magallon S (2010) Using fossils to break long branches in molecular dating: A comparison of relaxed clocks applied to the origin of angiosperms. *Syst Biol* 59:384–399.
7. Gernandt DS, et al. (2008) Use of simultaneous analyses to guide fossil-based calibrations of pinaceae phylogeny. *Int J Plant Sci* 169:1086–1099.
8. Farjon A (2005) *A Monograph of Cupressaceae and Sciadopitys* (Royal Botanic Gardens, Kew, UK), pp 47–53, 601–602.
9. Escapa I, Cúneo R, Axsmith B (2008) A new genus of the Cupressaceae (*sensu lato*) from the Jurassic of Patagonia: Implications for conifer megasporangiate cone homologies. *Rev Palaeobot Palyno* 151:110–122.
10. Rothwell GW, Stockey RA, Mapes G, Hilton J (2011) Structure and relationships of the Jurassic conifer seed cone *Hughmillerites juddii* gen. et comb. nov.: Implications for the origin and evolution of Cupressaceae. *Rev Palaeobot Palyno* 164:45–59.
11. Goloboff PA, Farris JS, Nixon KC (2008) TNT, a free program for phylogenetic analysis. *Cladistics* 24(5):774–786.
12. Near TJ, Meylan PA, Shaffer HB (2005) Assessing concordance of fossil calibration points in molecular clock studies: An example using turtles. *American Naturalist* 165:137–146.
13. McIver EE (2001) Cretaceous *Widdringtonia* Endl. (Cupressaceae) from North America. *Int J Plant Sci* 162:937–961.
14. Crisp MD, Cook LG (2011) Cenozoic extinctions account for the low diversity of extant gymnosperms compared with angiosperms. *New Phytol* 192:997–1009.
15. Rambaut A, Drummond AJ (2007) Tracer v1.4. Available at http://beast.bio.ed.ac.uk/Tracer.
16. Ho SY, Phillips MJ (2009) Accounting for calibration uncertainty in phylogenetic estimation of evolutionary divergence times. *Syst Biol* 58:367–380.
17. Near TJ, Sanderson MJ (2004) Assessing the quality of molecular divergence time estimates by fossil calibrations and fossil-based model selection. *Philos Trans R Soc Lond B Biol Sci* 359:1477–1483.
18. Near TJ, Bolnick DI, Wainwright PC (2005) Fossil calibrations and molecular divergence time estimates in centrarchid fishes (Teleostei: Centrarchidae). *Evolution* 59:1768–1782.
19. Davis CC, Schaefer H (2011) Plant evolution: Pulses of extinction and speciation in gymnosperm diversity. *Curr Biol* 21(24):R995–R998.
20. Linder HP, Hardy CR, Rutschmann F (2005) Taxon sampling effects in molecular clock dating: An example from the African Restionaceae. *Mol Phylogenet Evol* 35: 569–582.
21. Ree RH, Smith SA (2008) Maximum likelihood inference of geographic range evolution by dispersal, local extinction, and cladogenesis. *Syst Biol* 57:4–14.
22. Tiffney BH (1985) The Eocene North-Atlantic Land-Bridge: Its importance in tertiary and modern phytogeography of the Northern Hemisphere.2. *J Arnold Arboretum* 66: 243–273.
23. Scotese CR (2001) *Atlas of Earth History* (Department of Geology, University of Texas, Arlington, TX).
24. Morley RJ (2003) Interplate dispersal paths for megathermal angiosperms. *Perspect Plant Ecol Evol Syst* 6:5–20.
25. Smith AG, Smith DG, Funnell BM (2004) *Atlas of Cenozoic and Mesozoic Coastlines* (Cambridge University Press, Cambridge, UK).
26. Clayton JW, Soltis PS, Soltis DE (2009) Recent long-distance dispersal overshadows ancient biogeographical patterns in a pantropical angiosperm family (Simaroubaceae, Sapindales). *Syst Biol* 58:395–410.
27. Crisp MD, Trewick SA, Cook LG (2011) Hypothesis testing in biogeography. *Trends Ecol Evol* 26:66–72.
28. Ogg JG (2010) International Stratigraphic Chart (International Commission on Stratigraphy, West Lafayette, IN) Available at https://www.seegrid.csiro.au/wiki/pub/CGIModel/GeologicTime/StratChart2010.jpg.
29. Stadler T (2011) Simulating trees on a fixed number of extant species. *Syst Biol* 60: 676–684.
30. Cusimano N, Stadler T, Renner SS (2012) A new method for handling missing species in diversification analysis applicable to randomly or non-randomly sampled phylogenies. *Syst Biol*, 10.1093/sysbio/sys031.

Fig. S1. Maximum likelihood trees based on (*A*) the 56-taxon dataset (nuclear ribosomal DNA regions: 18S, 26S; mitochondrial DNA regions: *cox*I, *atp*A; plastid DNA regions: *rbc*L, *mat*K, *psb*B, *pet*B-D, *rps*4, and *trn*L-F) and (*B*) the 144-taxon dataset (plastid DNA regions only: *rbc*L, *mat*K, *psb*B, *pet*B-D, *rps*4, and *trn*L-F). Strongly supported nodes are marked by asterisks. A black asterisk indicates parsimony bootstrap support (PBS) ≥85% and Bayesian posterior probability (BPP) ≥0.98; a blue asterisk indicates PBS ≥85% but BPP <0.98; an orange asterisk indicates BPP ≥0.98 but PBS <85%.

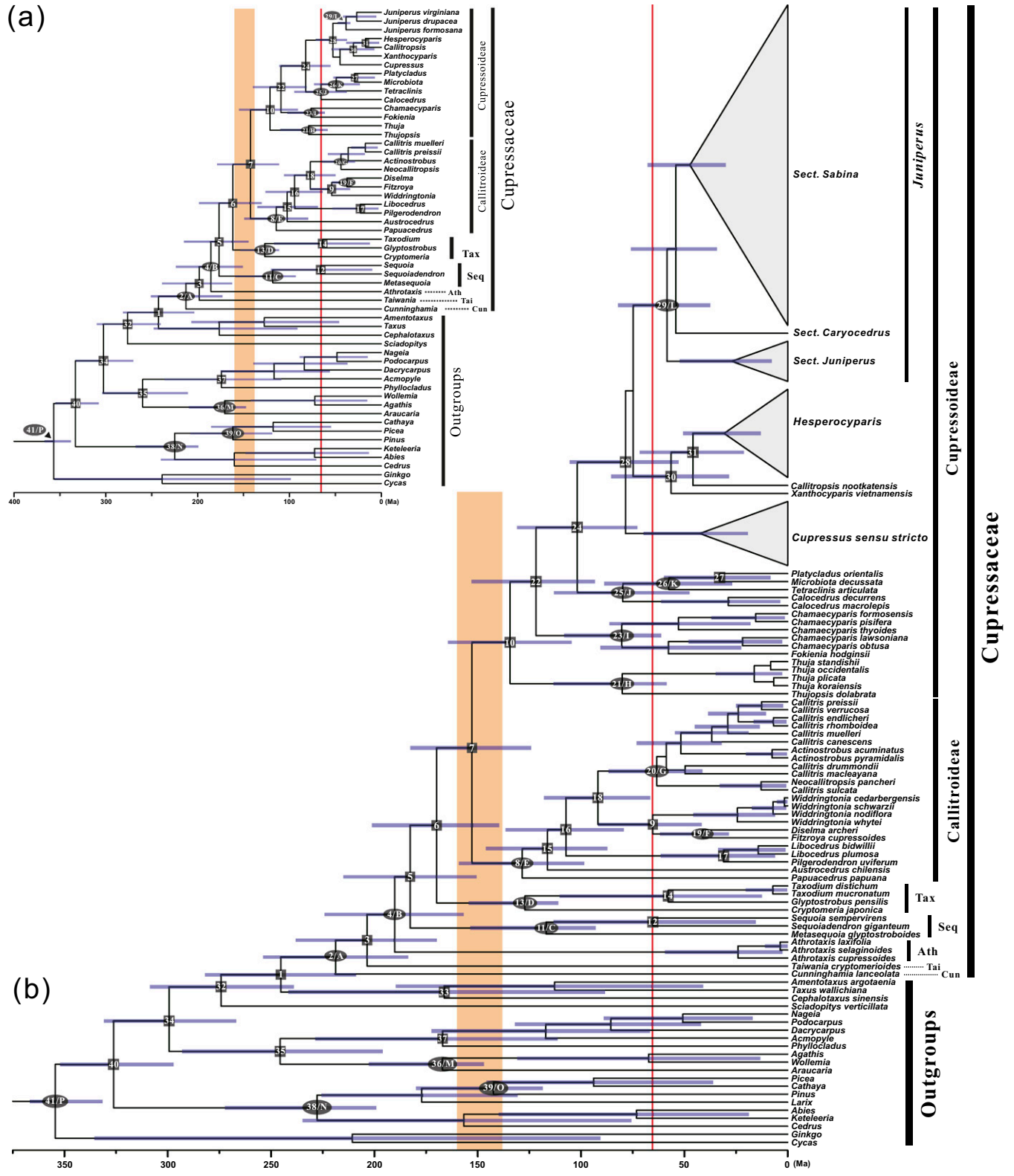

Fig. S2. Divergence times for the Cupressaceae based on (*A*) the 56-taxon dataset and (*B*) the 144-taxon dataset, with fossil calibration points and key nodes indicated. Light blue bars represent 95% highest posterior density intervals for age estimates. The red line indicates the Cretaceous/Tertiary boundary. Light orange shading represents the breaking up of Pangea into Laurasia and Gondwana.

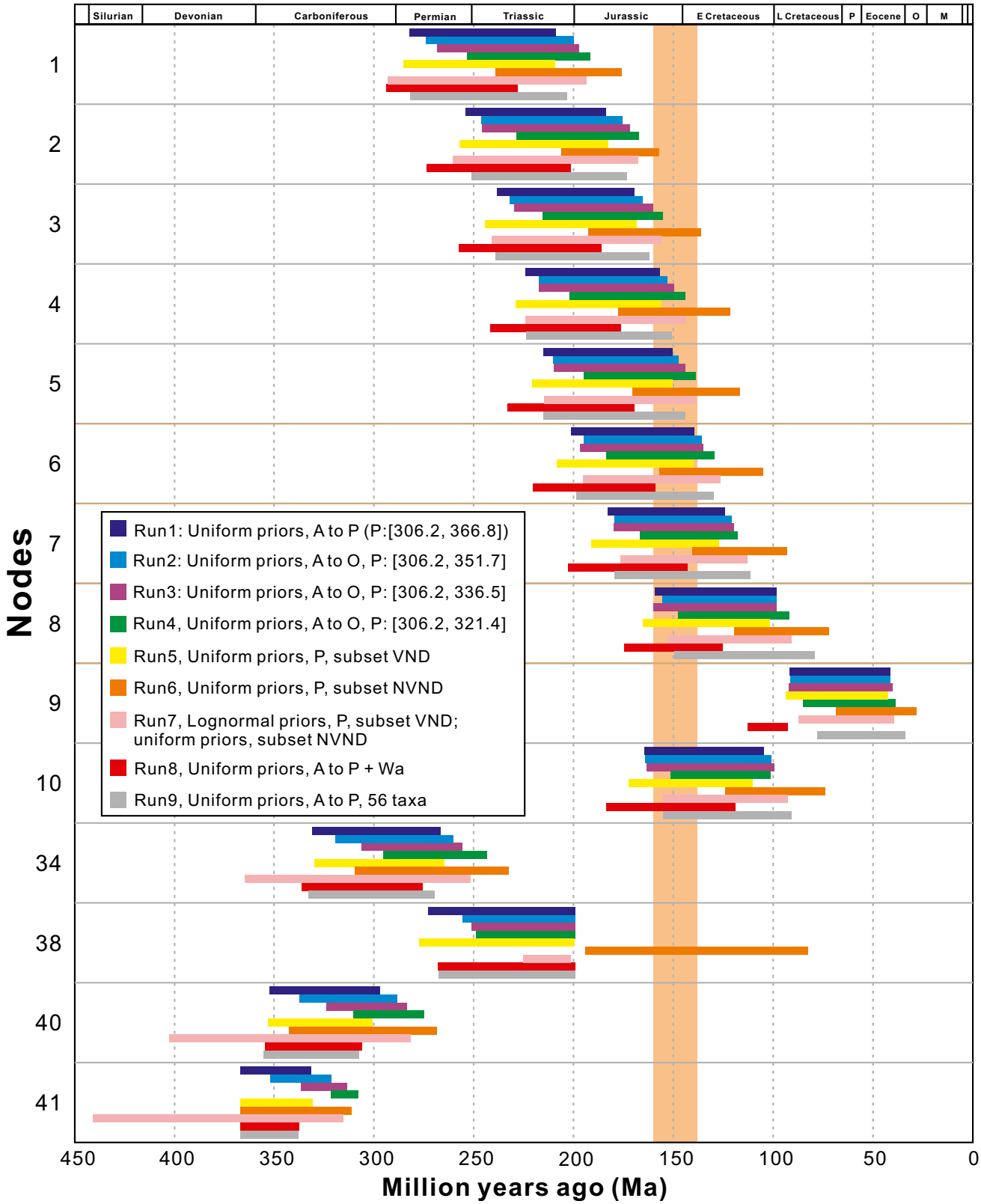

Fig. S3. Divergence time estimates for nodes 1–10 (see node descriptions in Table 1), the crown of Conifer clade II (node 34), Pinaceae (node 38), Conifers (Node 40), and Acrogymnospermae (Node 41) obtained with different calibration schemes and datasets. Gray bars represent age estimates from the 56-taxon dataset; bars of other colors represent age estimates from the 144-taxon dataset. Pink bars represent age estimates with lognormal priors for a subset of calibrations; bars of other colors represent age estimates with uniform priors. Gray and dark-blue bars represent age estimates with calibrations A through P (Table S4); light-blue, purple, and green bars represent age estimates with calibrations A through O, with the age ranges for calibration P constrained to [306.2, 351.7], [306.2, 366.5], or [306.2, 321.4] Ma. Yellow bars represent age estimates with calibration P plus calibrations C, D, H, I, M, N, and O (subset VND). Orange

Legend continued on following page

bars represent age estimates with calibration P and calibrations A, B, E, F, G, J, K, and L (subset NVND). Red bars represent age estimation with calibrations A–P and Wa. Pink bars represent age estimate with calibration P and subset VND set as lognormal priors and calibration subset NVND set as uniform priors. Light orange shading represents the breaking-up of Pangea into Laurasia and Gondwana.

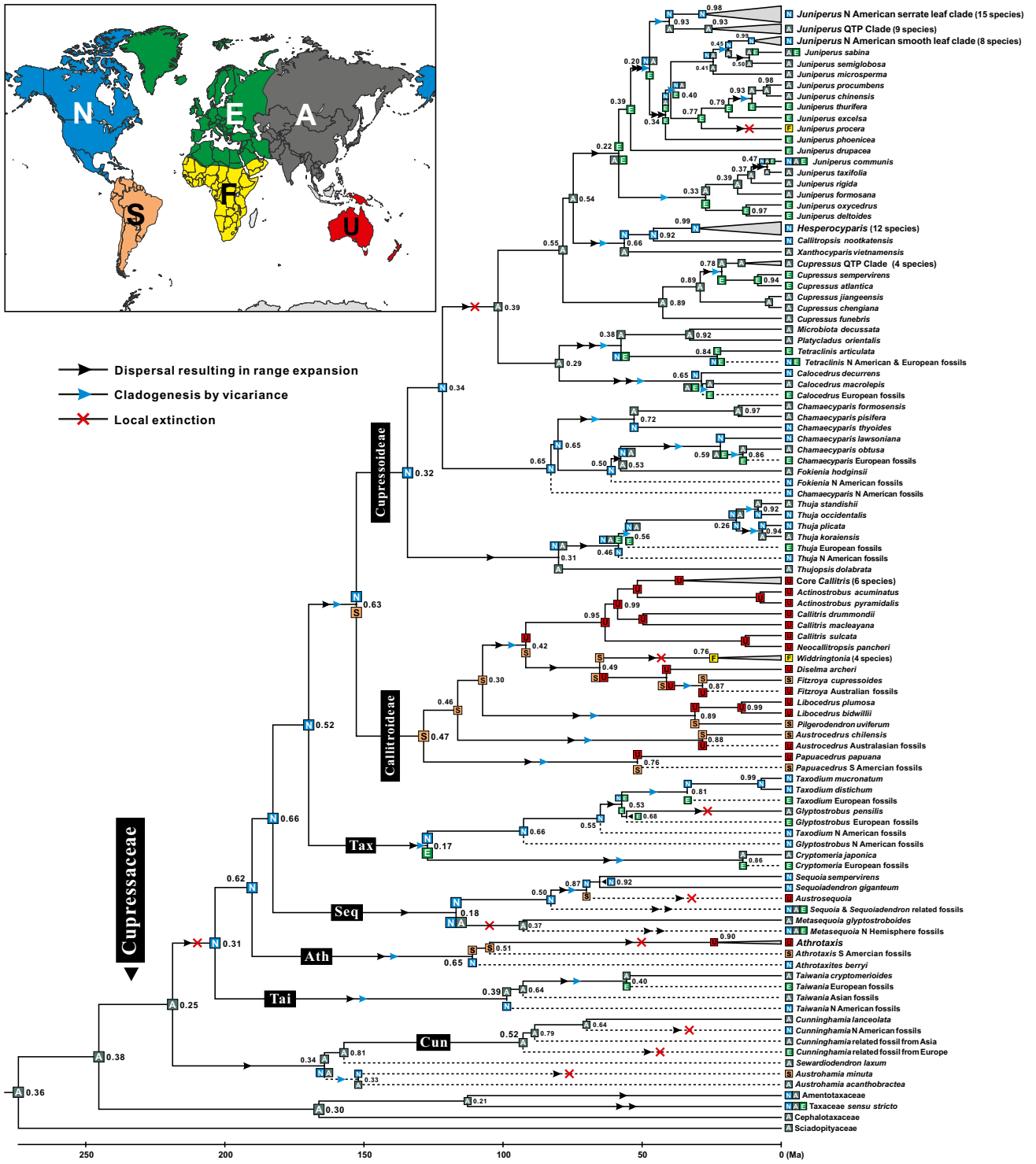

Fig. S4. The likelihood-based AAR for living and extinct members of Cupressaceae, which is the basis for Fig. 2*C* (scenario 1 in *SI Text*). (*Right*) The AARs with the highest likelihood are shown as colored boxes at each node. (*Left*) The six areas used in the analyses and the modeled biogeographic processes. Single-area boxes indicate an ancestor confined to a single geographic area; combined boxes indicate an ancestor with a distribution encompassing two or more areas; two boxes separated by a space indicate the ancestral ranges inherited by each of the daughter lineages arising from the respective ancestor. For nodes with alternative reconstructions (within log2 likelihood units of the maximum), the relative probability of the global likelihood for the optimal reconstruction is given. Extinct lineages known from fossils are indicated by dashed lines.

Fig. S5. Strict consensus trees reconstructed using a total-evidence approach (*SI Text*). (*A*) Plot shows phylogenetic positions of *Compsostrobus neotericus, Pityostrobus bernissartensis*, and *Araucaria mirabilis*. (*B–H*) Plots illustrate phylogenetic positions of *Hughmillerites juddii*, *Athrotaxis ungeri*, *Austrosequoia wintonensis*, *Glyptostrobus* sp., *Thuja polaris*, *Papuacedrus prechilensis*, and *Fokienia ravenscragensis*. (*I*) Plot shows the phylogenetic positions of the remaining 10 Cupressaceae fossils. Extinct lineages known from fossils are indicated by dashed lines, and their names are highlighted on a gray background.

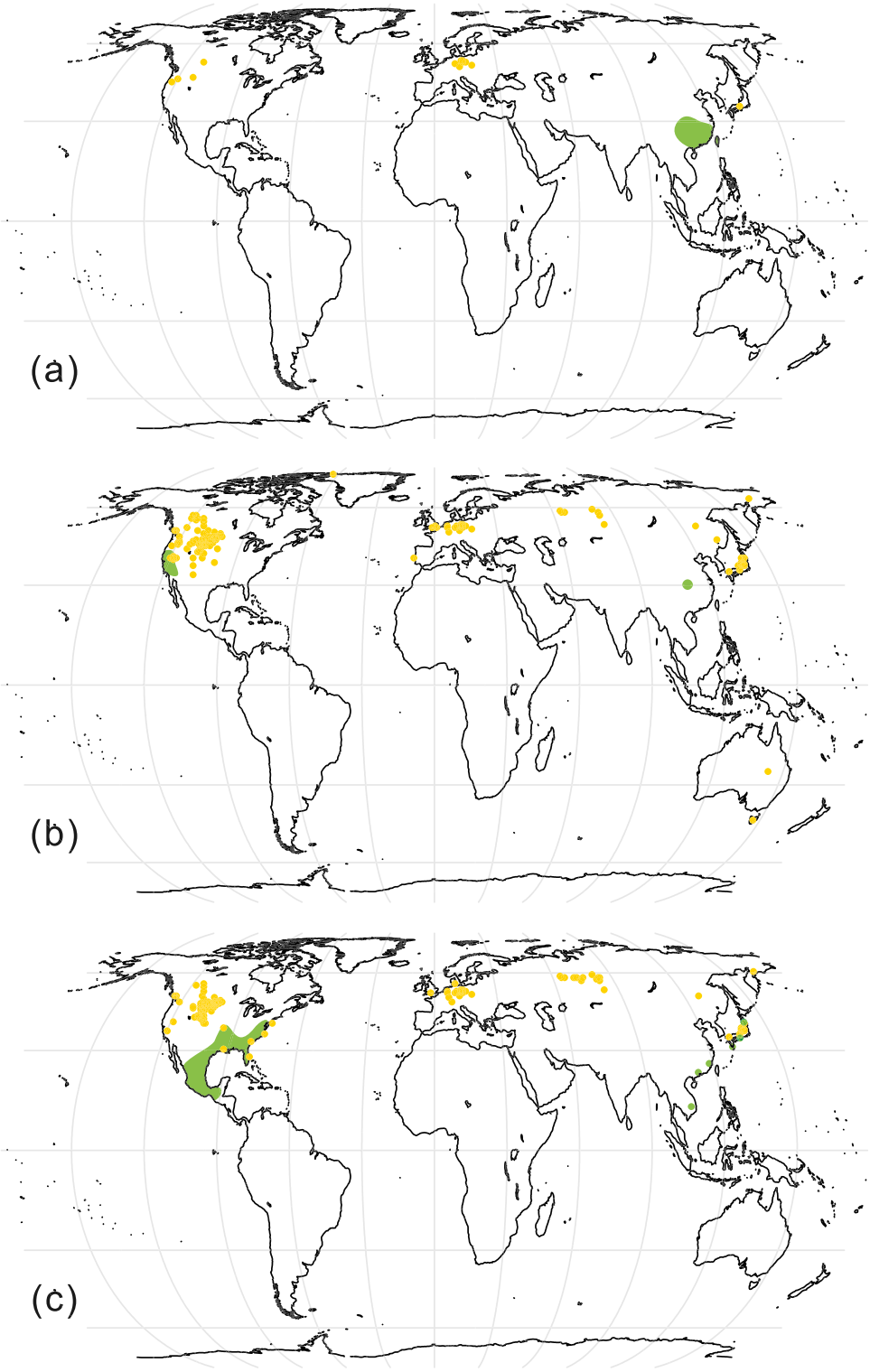

Fig. S6. Distributions of fossil (yellow solid circles) and living (green shading or green solid circles) Cupressaceae. (*A*) Cunninghamioideae. (*B*) Sequoioideae. (*C*) Taxodioideae. All three subfamilies underwent range contraction over time. Fossil distribution maps were compiled from the Paleobiology Database (http://paleodb.org).

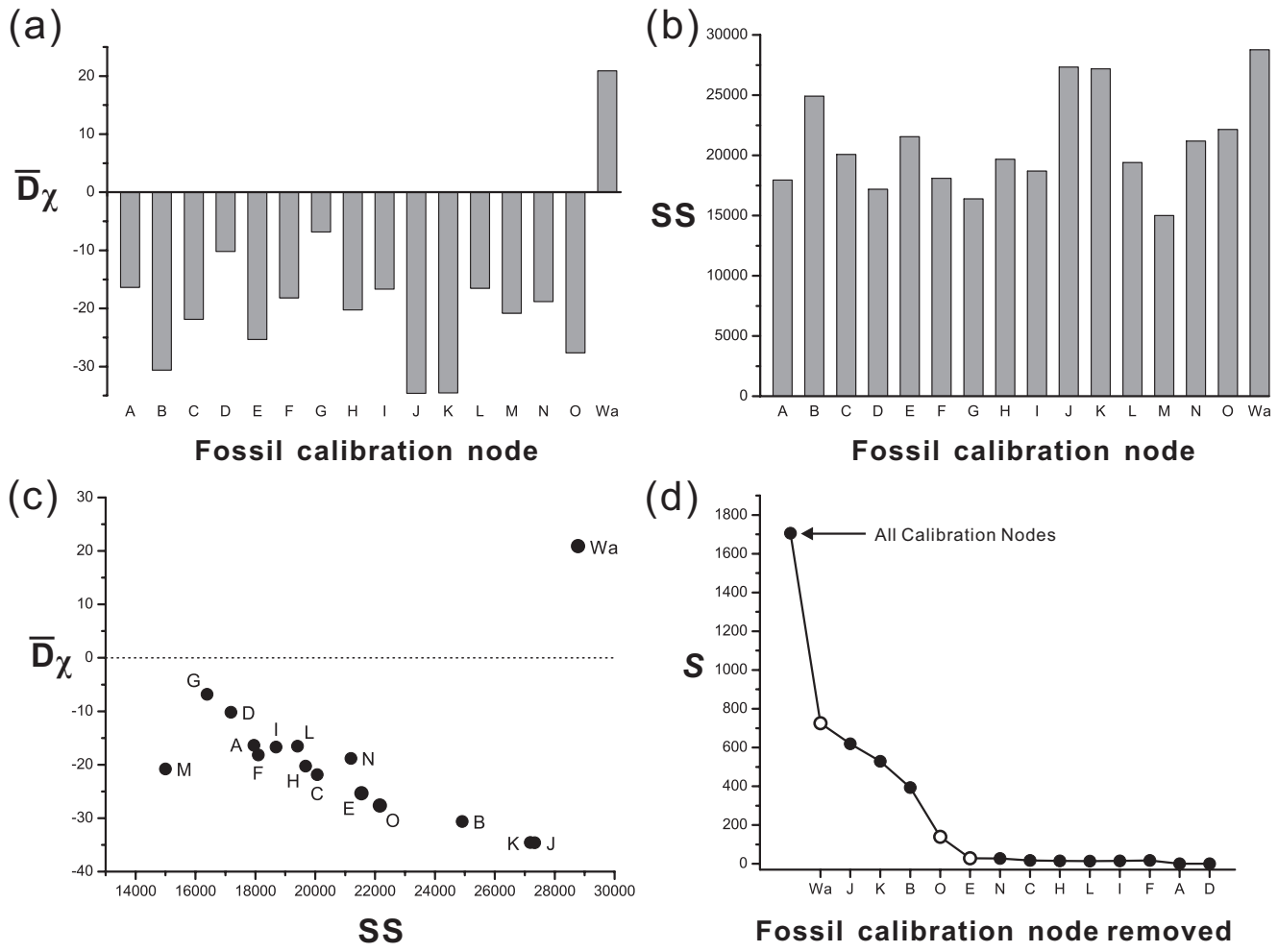

Fig. S7. Cross-validation of fossil calibrations A–O and Wa (Table S4) based on the 56-taxon dataset. (*A*) Histogram of the mean deviation ($\bar{D}$) (1) between molecular and fossil age estimates for all nodes, using a single fossil-dated node as a calibration point. (*B*) Histogram of the SS values (1) for a given fossil calibration node when it was used as the sole calibration point. (*C*) 2D plot for a given fossil calibration node with SS values (the sum of the squared differences between the molecular and fossil age estimates at all other fossil-dated nodes) (1) on the *x* axis and the mean deviation on the *y* axis. (*D*) Plot illustrating the effect on *s* (an average squared deviation for the deviation between molecular and fossil age estimates for all fossil calibrations in the analysis) of removing fossil calibration points (1). Open points indicate that the removal of the respective fossil calibration resulted in a significant reduction in the variance of *s*, based on a one-tailed Fisher's test (1). A maximum constraint of 366.8 Ma was placed on the older bound of calibration point P based on the arguments provided in Table S4.

1. Near TJ, Meylan PA, Shaffer HB (2005) Assessing concordance of fossil calibration points in molecular clock studies: an example using turtles. *Am Nat* 165:137–146.

Other Supporting Information Files

Table S1 (DOC)
Table S2 (DOC)
Table S3 (DOC)
Table S4 (DOC)
Table S5 (DOC)
Table S6 (DOC)